Sciencexpress Research Article

Radiocarbon Variability in the Western North Atlantic During the Last Deglaciation

Laura F. Robinson,[1]* Jess F. Adkins,[1] Lloyd D. Keigwin,[2] John Southon,[3] Diego P. Fernandez,[1] S-L Wang,[1] Daniel S. Scheirer[4]

[1]California Institute of Technology, MS 100-23, 1200 East California Boulevard, Pasadena, CA 91125, USA. [2]McLean Lab, Department of Geology and Geophysics, Woods Hole Oceanographic Institution, Woods Hole, MA 02543, USA. [3]Earth System Science Department, 3200 Croul Hall, University of California, Irvine, CA 92697–3100, USA. [4]U.S. Geological Survey, 345 Middlefield Road, MS989, Menlo Park, CA 94025, USA.

*To whom correspondence should be addressed. E-mail: laurar@gps.caltech.edu

We present a detailed history of glacial to Holocene radiocarbon in the deep Western North Atlantic from deep-sea corals and paired benthic-planktonic foraminifera. The deglaciation is marked by switches between radiocarbon enriched and depleted waters, leading to large radiocarbon gradients in the water column. These changes played an important role in modulating atmospheric radiocarbon. The deep-ocean record supports the notion of a bi-polar seesaw with increased Northern-source deep water formation linked to Northern Hemisphere warming and the reverse. By contrast, the more frequent radiocarbon variations in the intermediate/deep ocean are associated with roughly synchronous changes at the poles.

The last deglaciation was punctuated by numerous distinct millennial-scale climate events (*1*, *2*) and understanding the mechanisms behind these changes is a major goal of paleoceanography. The deep ocean stores and transports heat and carbon, so changes in its circulation are likely to influence global climate. Indeed, alternating the main site of deep water formation between the Northern and Southern hemispheres has been linked to switches in the amount of cross-equatorial heat transport (*3*). This bi-polar seesaw predicts sizable changes in mass transport in the deep North Atlantic and may be the cause of anti-phase warm and cool periods observed in Greenland and Antarctic ice-cores during the last deglaciation (*1*, *2*) (Fig. 1). Well-dated, high-resolution records are needed to make a mechanistic connection between deep-ocean circulation and climate. Passive geochemical tracers from marine sediments show us that during the last glacial maximum (LGM) Northern-source water (NSW) overlay Southern-source water (SSW) with the boundary at ~2,000m in the western North Atlantic (*4*, *5*). The transition from the LGM to the modern state, where North Atlantic Deep Water (NADW) dominates the Western basin, was marked by a series of changes in the deep-ocean circulation pattern (*6*, *7*). To help characterize those changes more completely, we have made $^{14}C/^{12}C$ measurements of well-dated samples of the deep-sea coral *Desmophyllum dianthus* (*8*).

A radiocarbon-age can be deduced for a given water mass if its radiocarbon content (^{14}C 5,730 year half-life) is known both when it forms, and when it reaches the deep ocean. By making depth profiles of $\Delta^{14}C$ in the past we can investigate variability in deep-ocean $\Delta^{14}C$ values, and begin to put constraints on changes in ocean circulation. Deep-sea radiocarbon records can also be used to investigate the role of the ocean in modulating the atmospheric carbon reservoir. The ocean contains ~60 times more carbon than the atmosphere, so small changes in uptake or release of radiocarbon from the ocean may cause significant changes in atmospheric $\Delta^{14}C$. Today, radiocarbon-enriched NADW formation draws down atmospheric ^{14}C more efficiently than radiocarbon-depleted Antarctic Bottom Water (AABW) formation, so varying the proportion of NSW to SSW, or changing the flux of NSW are both likely to change atmospheric $\Delta^{14}C$. Our record of ocean $\Delta^{14}C$ lets us constrain the influence of the deep ocean on atmospheric radiocarbon.

Using radiocarbon as a circulation tracer has been successful in the modern ocean. NADW and AABW have end-member values of –65 ‰ and –165 ‰ respectively (*9*–*11*). Radioactive decay causes deviations below the mixing line of these two end-members, allowing us to calculate the radiocarbon age of the water in the North Atlantic (*12*). In the modern Western North Atlantic (GEOSECS Station 120, 33°16'N) the water column has a small vertical $\Delta^{14}C$ gradient (~10 ‰ /1,000m) consistent with a single, Northern-source water mass (*13*). By contrast, further South in the Atlantic, NADW is underlain by Southern-sourced AABW. AABW has a characteristic low $\Delta^{14}C$ because the "old" Pacific intermediate water from which it forms is not at the surface long enough to re-equilibrate with the atmosphere. In the past, this approach is complicated by variability in the two end-member $\Delta^{14}C$-values at the sites of deep water formation

(*14*). For example, increasing the extent of sea-ice cover would allow less air-sea gas exchange, and, therefore, less radiocarbon in AABW. Constraints on the past deep-ocean $\Delta^{14}C$ have been acquired using the radiocarbon ages of planktonic and benthic foraminifera (BF-PF) and the aragonitic skeletons of deep-sea corals. In the foraminifera, the planktonic age can be converted to a calendar age, and the benthic $^{14}C/^{12}C$ ratio can then be used to calculate deep-ocean $\Delta^{14}C$. Early $\Delta^{14}C$ reconstructions suffered from problems of species-dependent age variability in planktonic $^{14}C/^{12}C$ measurements (*15–18*), but this problem is alleviated by targeting depths with high foraminiferal abundances or high sedimentation rates (*19*).

Deep-sea corals, typically found at water depths of ~500 to 2,500 m are datable by U-Th techniques and are good archives of palaeo-$\Delta^{14}C$ (*20–24*). Individual corals with different calendar ages can be compared to one another to give a resolution similar to that of ocean sediment cores. The solitary coral *D. dianthus* is thought to have a life span of ~100 years (*25*) so each individual skeleton can be sub-sampled for $^{14}C/^{12}C$ to construct decadal-resolution records of radiocarbon variability, comparable to the temporal resolution of ice core climate records (*20*). We collected more than 3,700 *D. dianthus* corals from the New England Seamounts in May 2003 (*26*). U-Th isotopic measurements were made by isotope dilution and 27 samples were selected for $^{14}C/^{12}C$ analysis (*27*) (table S1). Nine of these corals were sub-sampled to produce high-resolution transects of $\Delta^{14}C$. Our second sample set consists of 12 BF-PF pairs (spanning 19.5 ka to 10.7 ka) from the western North Atlantic and one additional sample using a benthic bivalve found in the core (table S2). Combining these data with published deep-sea corals and BF-PF pairs (*19*, *20*, *28–32*) allows us to reconstruct a detailed history of radiocarbon from the last glacial through to the Holocene.

Discussion. The ^{14}C content of the atmosphere and deep-sea are coupled, but our knowledge of the history of these two reservoirs is vastly different. The history of radiocarbon variability in the atmosphere is reasonably well constrained through the LGM and beyond (*33–35*). Radiocarbon and ^{10}Be are produced in the upper atmosphere simultaneously, and because ^{10}Be is not subject to decay or uptake in the carbon cycle, it can be used as a proxy for the ^{14}C production rate alone (*36*). Muscheler et al. (*36*) estimate the ^{10}Be production rate from the measured ^{10}Be content of Greenland ice cores, and convert it to an expected atmospheric $\Delta^{14}C$ record assuming that the present day carbon cycle was the same throughout (hereafter referred to as modelled atmospheric $\Delta^{14}C$) (Fig. 1) (*37*, *38*). Changes in observed atmospheric $\Delta^{14}C$ which are greater than predicted from the production rate curve alone must be due to deviations from the assumed modern steady-state, implying changes in the deep-ocean uptake on this 10^3 to 10^4 year time scale (*34– 36*). Compared to the atmosphere, our knowledge of the deep-ocean is more limited, both in depth and time. Our data fill this knowledge gap, allowing us to compare $\Delta^{14}C$ at depth intervals in the Western North Atlantic directly to the changes observed in the atmosphere (Fig. 2). A contour plot of the history of oceanic radiocarbon relative to atmospheric radiocarbon provides a true-age chronology through the glacial and deglacial periods (Fig. 3). It is clear from this plot that intermediate-deep (I/D, 1,700 m to 2,500 m) waters are more variable than the abyss. A horizontal $\Delta^{14}C$ divide separates water masses above and below ~2,500m, and NSW penetrates below this divide only twice during the deglaciation. A deglacial, radiocarbon-depleted, I/D water mass (akin to modern Antarctic Intermediate Water) is present at 40°N during Heinrich 1, 15.4 ka and the Younger Dryas.

Glacial Ocean. From 28 to 17 ka, the $\Delta^{14}C$ of the Western North Atlantic is constrained by 12 points (11 BF-PF pairs and 1 coral) (Fig. 2A). The 25 ka coral at 1,700m has a $\Delta^{14}C$ only 66 ‰ lower than the atmosphere, indicative of well-ventilated NSW. By contrast, all deeper samples are more depleted in radiocarbon than anywhere in the modern ocean. This depletion is >400 ‰ at 28 ka and drops to ~230 ‰ during the LGM (arrows a and b, Fig. 2A and Fig. 4A). A slow down in the ventilation rate, or a change in the proportion of NSW to SSW may account for some of this observed $\Delta^{14}C$ shift in the deep ocean. However, Cd/Ca ratios show us that the LGM deep North Atlantic was filled by SSW (*6*), and the pattern of deep-sea $\Delta^{14}C$ from 21 to 18.7 ka reflects the atmosphere nearly synchronously, suggesting that this SSW water was circulating vigorously (*39*) (Fig. 2a). An alternative likely cause of radiocarbon depletion in the Southern Ocean is extensive sea-ice coverage which would reduce amount of the air-sea carbon exchange. In support of this mechanism, diatom based reconstructions show that the LGM sea-ice extent was 5° further North than at the present day and that before the LGM the sea-ice exhibited less seasonal variability (*40–42*). Over the same time period, 30 ka-LGM, the observed and modelled $\Delta^{14}C$ of the atmospheric records converged from a large offset of >350 ‰ to ~250 ‰ (arrows a and b, Fig. 1). We suggest that the reduction in the atmospheric ^{14}C content was caused by an increase in the ^{14}C uptake in the Southern Ocean. Not only would such a change in the Southern Ocean affect the $\Delta^{14}C$ of North Atlantic water but, as the dominant source to the deep Pacific, it could alter the whole ocean ^{14}C inventory.

Heinrich 1 and the 15.4 ka event. Heinrich events are characterised by massive ice-rafted debris (IRD) deposits in the North Atlantic (*43*), and it has been suggested that these large freshwater inputs in the Northern hemisphere may

reduce the rate of Northern-sourced deep-water formation by lowering the density of surface water. The (Pa/Th) ratio of a marine sediment record from 4,500m at the Bermuda Rise shifts towards values indicative of such a reduction during Heinrich 1 (*44*). As expected, this slow down in NSW flux is consistent with a reduction in the amount of uptake of ^{14}C by the deep Atlantic, and a divergence in the modelled and observed atmospheric records (Fig. 1, arrow c), although the signal is not large.

During Heinrich 1 the $\Delta^{14}C$ water column profile is characterised by radiocarbon-rich water overlying radiocarbon-poor water (Fig. 4A) indicative of a greater proportion of SSW deeper in the water column. This deep water in the North Atlantic has the same offset from the atmosphere as the Southern Source end-member (~265 ‰, constrained by a 16.7 ka deep-sea coral from the Drake Passage) (*21*) implying a vigorous deep SSW circulation. These radiocarbon data are not consistent with the Bermuda Rise (Pa/Th) record (*44*) if the latter is interpreted as a dramatic reduction of deep-water ventilation rate. On the other hand, our data show the $\Delta^{14}C$ of I/D water decreasing through Heinrich 1, consistent with a reduction in NSW flux (Fig. 2B). Six coral individuals describe a "U-shaped" change in $\Delta^{14}C$ in the I/D ocean beginning at 16.3 ka (Fig. 2B, arrow x). Multiple measurements from within one coral at 2,000m define a $\Delta^{14}C$ decrease of 50 ‰ in ~100 years (Fig 2B). This decrease occurred faster than the rate of ^{14}C decay, and so must be due, at least in part, to mixing-in of low $\Delta^{14}C$ SSW. This downward trend reverses at 16.2 ka, when multiple ^{14}C measurements within a second coral define a 30 ‰ rise in $\Delta^{14}C$, caused by an increase in the influence of radiocarbon-rich NSW (Fig. 2B). The timing of the turn in the $\Delta^{14}C$-U-shape, 16.2 ka, is coincident with the start of the dramatic decrease in $\Delta^{14}C$ observed in the atmosphere (within calendar age error limits) and signals the end of Heinrich 1 at I/D depths.

After Heinrich 1, at 15.5 ka, all corals from 1,700 to 2,500 m have a $\Delta^{14}C$ signal ~100 ‰ lower than the atmosphere, indicative of a well-mixed, well-ventilated, Northern-source I/D water column. Deeper, at 3,500m, SSW still fills the deep water column as shown by a BF-PF pair with a 250‰ offset from the atmosphere (Fig. 2B).

The modelled and observed atmospheric $\Delta^{14}C$ records converge after Heinrich 1. This convergence is interrupted by a plateau in the atmospheric $\Delta^{14}C$ record that last from ~15.7 ka to 15.0 ka and is coincident with a pause in the deglacial temperature rise in both hemispheres (arrow y, Fig. 1). At water depths of 1,700 to 2,000 m, this 15.4 ka event is characterised by a massive and rapid (100 ‰ in ~100 years) drop in $\Delta^{14}C$ (*20*) (Fig. 2B, arrow y). Multiple ^{14}C measurements within the lifetime of each of four individual corals from two different seamounts clearly define this trend. The decrease is much faster than *insitu* decay of ^{14}C and must be due to mixing-in of low $\Delta^{14}C$ SSW. A $\Delta^{14}C$ decrease is also seen at 2,500m, but with a lesser amplitude (~40 ‰). We interpret this change as a ^{14}C-depleted front spreading northward, rather than a shoaling of deeper water, because the $\Delta^{14}C$ is lower at 2,000m than at 2,500m. This increase in the volume of I/D SSW at the expense of ^{14}C rich NSW formation at the 15.4 ka event is the likely cause of the ^{14}C plateau in the atmosphere.

At the end of the 15.4 ka event, the water column has an "inverted" profile with radiocarbon-poor water overlying radiocarbon-rich water (Figs. 2B and 4A). This inverted profile is analogous to GEOSECS profiles further South in the modern West Atlantic, although the gradients are much smaller in the modern ocean. Deglacial intermediate SSW masses have previously been observed in benthic $\delta^{13}C$ records at lower latitudes in the Tasman Sea and at the Chatham Rise (*45*, *46*) but this is the first time that water with such low $\Delta^{14}C$ is seen at I/D depths so far north.

Bolling-Allerod to Holocene. The Bolling begins at ~14.6 ka on the GISP2 timescale (*2*, *47*) and is widely recorded across the Northern Hemisphere (Fig. 1). Cd/Ca (*6*) and Nd isotopes (*48*), from the North and South Atlantic respectively show that NSW dominated the deep Atlantic during the Bolling. The modelled and observed $\Delta^{14}C$ records converge with one another at this time (arrow d, Fig. 1), suggesting that the Bolling-ocean was capable of drawing down as much radiocarbon as the modern carbon cycle. Consistent with this suggestion, we observe that the $\Delta^{14}C$ depth profile is more like the modern ocean than at any time since the glacial (*49*) (Fig. 4B). The entire water column is filled by radiocarbon-rich water, with deep water (3,500 m) only 70 ‰ lower than the atmosphere (Fig. 4B). Radiocarbon rich water also invaded the Eastern Atlantic at this time (*50*). The timing of this NSW flush is consistent with the reinvigoration of export from the North Atlantic as recorded by (Pa/Th) (*44*).
The end of the Bolling is characterised by cooling (Fig. 1) (*2*), and is coincident with a 700 year, 160 ‰ drop in deep-ocean $\Delta^{14}C$ at 3,500m (Fig. 2C) (*51*).The resulting Allerod water column $\Delta^{14}C$-profile is consistent with Cd/Ca ratios which indicate that the deep Atlantic was filled by a mix of NSW and SSW (*6*). This mixture was ~170 ‰ offset from the atmosphere as shown by BF-PF pairs from 3,500m (13.9 ka) and 4,250m (13.6 ka) and an equatorial deep-sea coral from 2,300m (~14.0 ka) (*23*, *24*). This reduction in the amount of deep NSW formation is the likely cause of the divergence of modelled and atmospheric $\Delta^{14}C$ records in the transition from the Bolling to the Allerod (Fig. 1).

The beginning of the Younger Dryas, at 12.9 ka, is characterised by a large decrease in Northern hemisphere temperature (Fig. 1). The $\Delta^{14}C$ depth profile is "inverted" between 1,700m and 2,500m (Fig. 4B (*20*, *28*) but at ~2,500m

there is a sharp transition back to radiocarbon-depleted deep water, ~300 ‰ offset from the atmosphere (Fig. 4B) (*19*). The increased proportion of radiocarbon-depleted SSW at I/D and abyssal depths is the likely cause of the marked divergence between the modelled and observed atmospheric $\Delta^{14}C$ records (Fig. 1, arrow e) (*34*, *52*). During the Younger-Dryas, at ~12 ka, Eltgroth et al. (*28*) report a $\Delta^{14}C$ "spike" at I/D water depths from corals on either side of the North Atlantic (New England Seamount (arrow z, Fig. 2C) and Azores). This transient flushing of well-ventilated NSW is synchronous with a kink in the atmospheric $\Delta^{14}C$ record and a brief warm event observed in both Antarctica and Greenland ice cores (arrow z, Fig. 1).

At the end of the Younger Dryas, 4 BF-PF pairs spanning 1,400m to 4,250m all have the same ~100 ‰ $\Delta^{14}C$ offset from the atmosphere (Fig. 3A). This final flush of radiocarbon-rich NSW fills the entire depth range of the Western Atlantic by 10.6 ka, drawing down ^{14}C and causing the modelled and observed atmospheric $\Delta^{14}C$ to converge. This overall circulation pattern and associated carbon cycle is similar to the modern day (arrow f, Fig. 1).

Conclusions. The deep-ocean radiocarbon pattern supports the notion of the bi-polar seesaw: when the deep ocean was flushed by radiocarbon-rich NSW Greenland was warming and when NSW was replaced by SSW Greenland was cooling. The I/D ocean is much more variable, with multiple switches between radiocarbon-depleted and enriched water masses (Fig. 3). These I/D-ocean radiocarbon events are associated with small climate changes observed in both Greenland and Antarctic ice cores. Increasing $\Delta^{14}C$ in the I/D ocean is associated with either no temperature change or with warming. Decreasing I/D ocean $\Delta^{14}C$ is associated with interruptions in the rise of temperature out of the LGM. This pattern is inconsistent with a bi-polar seesaw link between cross equatorial heat flux and climate change. I/D water mass variability does not have as large an effect on climate as deep-ocean variability, but may play an important role in modulating the atmospheric carbon reservoir.

References and Notes

1. R. B. Alley *et al.*, *Nature* **362**, 527 (1993).
2. T. Blunier, E. J. Brook, *Science* **291**, 109 (2001).
3. W. S. Broecker, *Paleoceanography* **13**, 119 (1998).
4. W. B. Curry, D. W. Oppo, *Paleoceanography* **20** (2005).
5. D. W. Oppo, S. J. Lehman, *Science* **259**, 1148 (1993).
6. E. A. Boyle, L. D. Keigwin, *Nature* **330**, 35 (1987).
7. T. M. Marchitto, Jr., W. B. Curry, D. W. Oppo, *Nature* **393**, 557 (1998).
8. *D. dianthus* and *D. Cristagalli* are two names for the same coral; the former is more widely used.
9. W. S. Broecker, S. Blanton, M. Smethie Jr., H. G. Ostlund, *Global Geochemical cycles* **5**, 87 (1991).
10. M. Stuiver, P. D. Quay, H. G. Ostlund, *Science* **219**, 849 (1983).
11. C. Wunsch, *Quaternary Science Reviews* **22**, 371 (2003).
12. W. S. Broecker, T. H. Peng, *Tracers in the sea* (Lamont-Doherty Geol. Obs.. Palisades NY United States, 1982).
13. M. Stuiver, H. G. Ostlund, *Radiocarbon* **22**, 1 (1980).
14. $^{14}C/^{12}C$ ratios are reported as $\Delta^{14}C$, the ratio of a sample to the pre-industrial pre- nuclear atmospheric standard in units of ‰.
15. W. Broecker *et al.*, *Radiocarbon* **30**, 261 (1988).
16. W. S. Broecker *et al.*, *Radiocarbon* **32**, 119 (1990).
17. J. C. Duplessy *et al.*, *Radiocarbon* **31**, 493 (1989).
18. N. J. Shackleton *et al.*, *Nature* **335**, 708 (1988).
19. L. D. Keigwin, *Paleoceanography* **19** (2004).
20. J. F. Adkins, H. Cheng, E. A. Boyle, E. R. M. Druffel, R. L. Edwards, *Science* **280**, 725 (1998).
21. S. J. Goldstein, D. W. Lea, S. Chakraborty, M. Kashgarian, M. T. Murrell, *Earth* and Planetary Science Letters **193**, 167 (2001).
22. N. Frank *et al.*, *Earth and Planetary Science Letters* **219**, 297 (2004).
23. A. Mangini *et al.*, *Nature* **392**, 347 (1998).
24. A. Schroder-Ritzrau, A. Mangini, M. Lomitschka, *Earth and Planetary Science Letters* **216**, 399 (2003).
25. J. F. Adkins, G. M. Henderson, S. L. Wang, S. O'Shea, F. Mokadem, *Earth and* Planetary Science Letters **227**, 481 (2004).
26. All corals in this study were collected in May 2003 using the deep submergence vehicle Alvin ensuring that the depth of each coral (between 1,100m and 2,500m) was well known, and the corals were collected at, or near to, life position. The Seamount locations are; Muir 33°30'N, 62°30'W, Manning ~38°0'N, 60°30'W, Gregg 39°0'N, 61°0'W.
27. Methods are available as supporting material on Science Online.
28. S. Eltgroth, J. F. Adkins, L. F. Robinson, J. Southon, M. Kashgarian, Paleoceanography (submitted).
29. L. D. Keigwin, M. A. Schlegel, *Geochemistry Geophysics Geosystems* **3**, AN1034 (2002).
30. L. D. Keigwin, J. P. Sachs, Y. Rosenthal, E. A. Boyle, *Paleoceanography* **20**, doi:10.1029/2004PA001074 (2005).
31. L. D. Keigwin, G. A. Jones, *Journal of Geophysical Research-Oceans* **99**, 12397 (1994).
32. L. D. Keigwin, G. A. Jones, S. J. Lehman, E. A. Boyle, *Journal of Geophysical Research-Oceans* **96**, 16811 (1991).
33. K. A. Hughen *et al.*, *Radiocarbon* **46**, 1059 (2005).
34. K. A. Hughen *et al.*, *Science* **303**, 202 (2004).
35. J. W. Beck *et al.*, *Science*, 2453 (2001).

36. R. Muscheler *et al.*, *Earth and Planetary Science Letters* **219**, 325 (2004).
37. After its initial production, ^{10}Be is attached to aerosols and removed from the atmosphere with a 1- to 2-year residence time. As this process is completely different than the ^{14}C removal mechanism, variations in the ratio of wet and dry deposition at Greenland could lead to ^{10}Be accumulation rate changes that are not correlated with cosmogenic radionuclide production rate changes. We do not consider this possible source of error in our analysis.
38. G. M. Raisbeck *et al.*, *Geophysical Research Letters* **8** (1981).
39. P. J. Reimer *et al.*, *Radiocarbon* **46**, 1029 (2005).
40. R. Gersonde *et al.*, *Paleoceanography* **18** (2003).
41. R. Gersonde, X. Crosta, A. Abelmann, L. Armand, *Quaternary Science Reviews* **24**, 869 (2005).
42. R. Gersonde, U. Zielinski, *Palaeogeography Palaeoclimatology Palaeoecology* **162**, 263 (2000).
43. S. R. Hemming, *Reviews of Geophysics* **42**, doi:10.1029/2003RG000128 (2004).
44. J. F. McManus, R. Francois, J. M. Gherardi, L. D. Keigwin, S. Brown-Leger, *Nature* **428**, 834 (2004).
45. H. C. Bostock, B. N. Opdyke, M. K. Gagan, L. K. Fifield, *Paleoceanography* **19**, PA4013 (2004).
46. K. Pahnke, R. Zahn, *Science* **307**, 1741 (2005).
47. P. M. Grootes, M. Stuiver, J. W. C. White, S. Johnsen, J. Jouzel, *Nature* **366**, 552 (1993).
48. A. M. Piotrowski, S. L. Goldstein, S. R. Hemming, R. G. Fairbanks, *Earth and* Planetary Science Letters **225**, 205 (2004).
49. Two new samples at 15.0 ka (1,180m) and 14.3 ka (1,221m) both from Gregg Seamount, have 26 ‰ and 0 ‰ offset from the atmosphere respectively. From the end of Heinrich 1 to ~14.2 ka, the atmospheric radiocarbon content dropped at least as fast as the decay rate leading to a situation where the decrease in the radiocarbon content of the atmosphere could "overtake" the decay rate in an isolated water mass. Two samples from the end of the Younger Dryas are also within error of the atmospheric value and lie at the end of a marked drop in the atmospheric radiocarbon content (28).
50. L. C. Skinner, N. J. Shackleton, *Paleoceanography* **19** (2004).
51. This trend is well constrained by 5 BF-PF pairs, three of which (including the oldest and youngest) are from the same core.
52. K. A. Hughen *et al.*, *Nature* **391**, 65 (1998).
53. R. G. Fairbanks *et al.*, *Quaternary Science Reviews* **24**, 1781 (2005).
54. Y. J. Wang *et al.*, *Science* **294**, 2345 (2001).
55. We would like to acknowledge The Comer Foundation for Abrupt Climate Change, The Henry Luce Foundation, The American Chemical Society Petroleum Research Fund and NSF Grant Numbers OCE-0096373 and OCE-0095331. We would also like to thank all members of the cruise AT7-35 to the New England Seamounts.

Supporting Online Material
www.sciencemag.org /cgi/content/full/1114832/DC1
Materials and Methods
Tables S1–S3
References and Notes

13 May 2005; accepted 24 October 2005
Published Online 3 November 2005;10.1126/science.1114832
Include this information when citing this paper.

Fig. 1. The top three curves are observed atmospheric Δ^{14}C records; Cariaco Basin in grey (*34*), a Bahamas speleothem in black (*35*) and Intcal04 in purple (*39*) which, during the main period of interest, is primarily based on precisely dated surface coral data (*53*). All of these records are in reasonable agreement from 10 ka back to ~15.5 ka, but there are differences during Heinrich 1. The age model for the Cariaco Basin is poorly constrained during Heinrich 1, with the exception of a distinct change in greyscale that matches a δ^{18}O event in both GISP2 and a U-Th dated speleothem from Hulu Cave (*54*) at 16.0 ka. Two outliers have been removed from the Cariaco record (16.10 ka and 17.96 ka). Between 26 and 22 ka we plot only the Intcal04 (*39*) and speleothem data (*35*) which are consistent with one another. When comparing our ocean Δ^{14}C data to the atmosphere we refer to Intcal 04 (*39*) except between 17.5 ka and 14.5 ka where there are no surface coral data and the record is poorly constrained. In this 3 kyr period we combine the Cariaco (*34*) and speleothem records (*35*) as our best estimate of the atmosphere. The ^{10}Be based Δ^{14}C (modelled) reconstruction is plotted on the same scale as the observed atmospheric record, with the maximum and minimum as thin lines, and the mean as a thick red line (*36*). Arrows a-f and x-z point to times that are referred to in the text. The GISP2 (green) and Byrd δ^{18}O (yellow) records are plotted after Blunier and Brook (*2*).

Fig. 2. Raw Δ^{14}C data for (**A**) glacial-LGM, (**B**) 16.4 to 15.1 ka, and (**C**) 15.1 to 10.0 ka compartmentalised into seven depth-bands; 1,176 to 1,221 m (red, circles), 1,381 to 1,400 m (orange, upside-down triangles), 1,713 to 1,790 m (black, squares), 1,886 to 2,155 m (pale blue, diamonds), 2,228 to 2,590 m (purple, triangles), 2,972 to 3,845 m (blue, crosses) and 4,055 to 4,712 m (green, stars) below sea level. Each record is plotted against calendar age BP with 2σ error ellipses. Open symbols are BF-PF pairs, closed symbols are corals. One published Younger Dryas BF-PF data point (*19*) is not plotted as it lies above the atmospheric curve. In Fig. 2B, color coded 2σ calendar age error bars are shown as

horizontal bars with error ellipses representing the relative error between individual points on the same coral. Solid lines join $\Delta^{14}C$ measurements from within one coral; dashed lines connect data from separate corals. Two coral data points (1,886 m, 16.1 ka and 2,500 m, 15.9 ka) are not shown as they have large calendar age errors that overlap other data points (242 and 297 years respectively). The two points with large error ellipses that are shown are BF-PF pairs.

Fig. 3. Cartoon contour plot for all coral (closed circles) and BF-PF (open circles) data from 26 to 10 ka and deeper than 1000m in the Western North Atlantic. Data is plotted relative to the atmospheric record shown in Fig. 1. Dark colours are low in radiocarbon and light colours are rich in radiocarbon. One BF-PF sample from 27.7 ka (*19*) lies off the time axis, it is from 2,972m and has a >400 ‰ offset from the atmosphere. Brackets at the bottom show the time intervals for the depth profiles in Fig. 4.

Fig. 4. Depth profiles of $\Delta^{14}C$ relative to the atmosphere in the ocean are chosen from discrete time slices from the glacial to modern (GEOSECS) (*13*). Open symbols are BF-PF pairs, closed symbols are corals. The data in each profile are bracketed in Fig. 3 and marked in table S3. These profiles are not representative of "steady-state" ocean configurations, but they are plotted to demonstrate the large and variable radiocarbon gradients in the deep and I/D ocean.

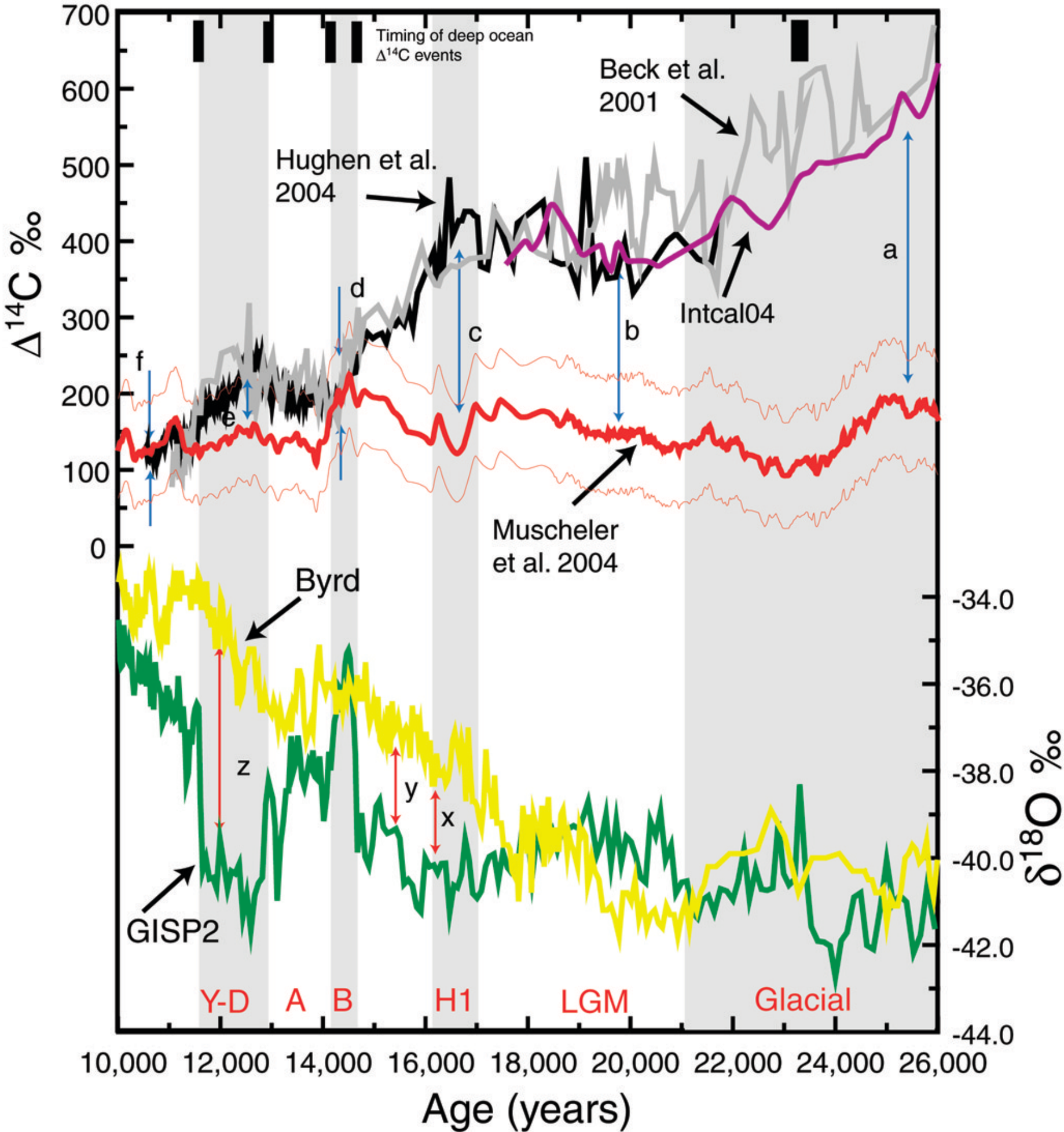
Timing of deep ocean
Δ14C events
Beck et al.
2001
Hughen et al.
2004
Intcal04
Muscheler
et al. 2004
Byrd
GISP2
a
b
c
d
e
f
x
y
z
Y-D
A
B
H1
LGM
Glacial
Δ14C ‰
δ18O ‰
Age (years)
700
600
500
400
300
200
100
0
-34.0
-36.0
-38.0
-40.0
-42.0
-44.0
10,000
12,000
14,000
16,000
18,000
20,000
22,000
24,000
26,000

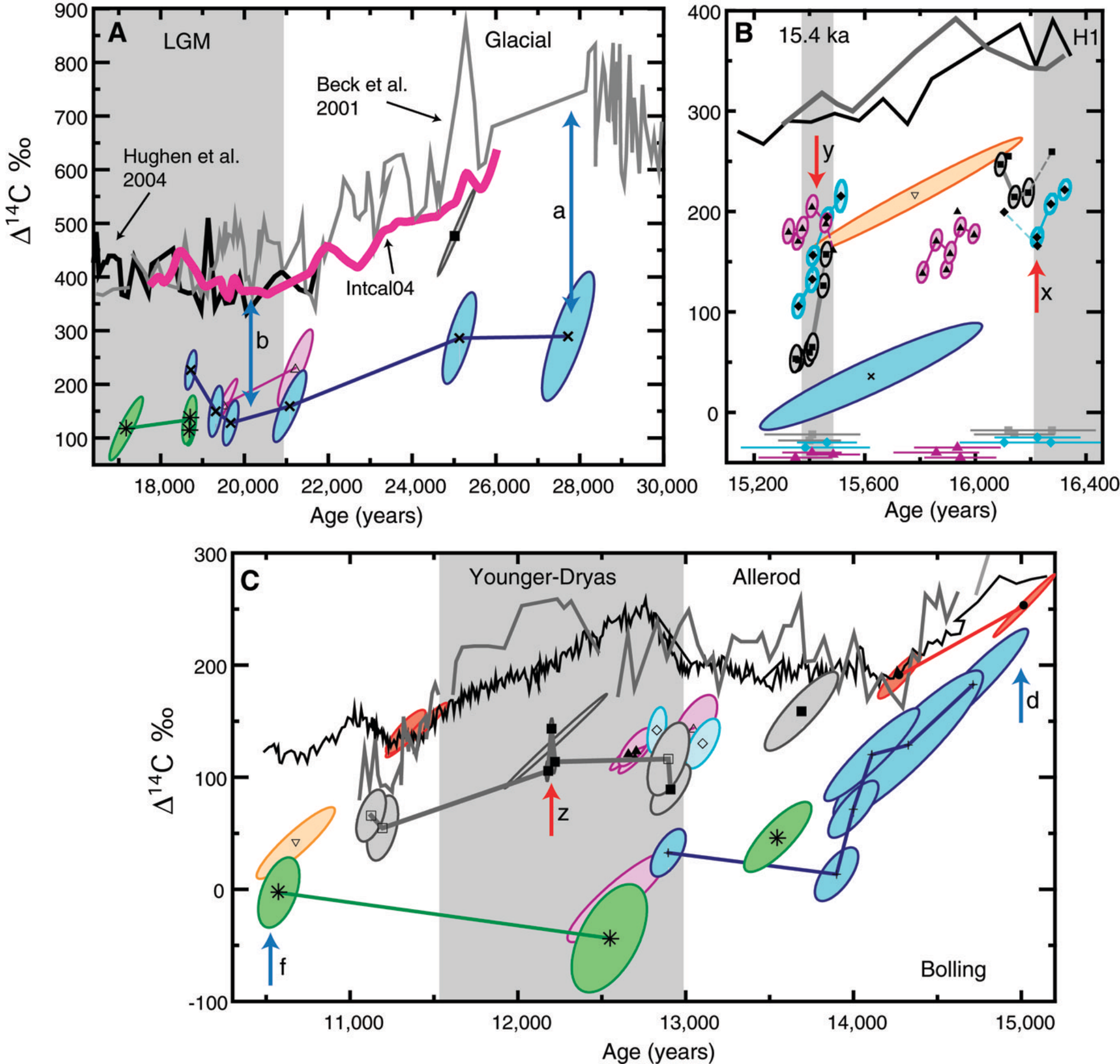
A
LGM
Glacial
Beck et al.
2001
Hughen et al.
2004
Intcal04
a
b
Δ14C ‰
Age (years)
B
15.4 ka
H1
y
x
Age (years)
C
Younger-Dryas
Allerod
Bolling
z
d
f
Δ14C ‰
Age (years)

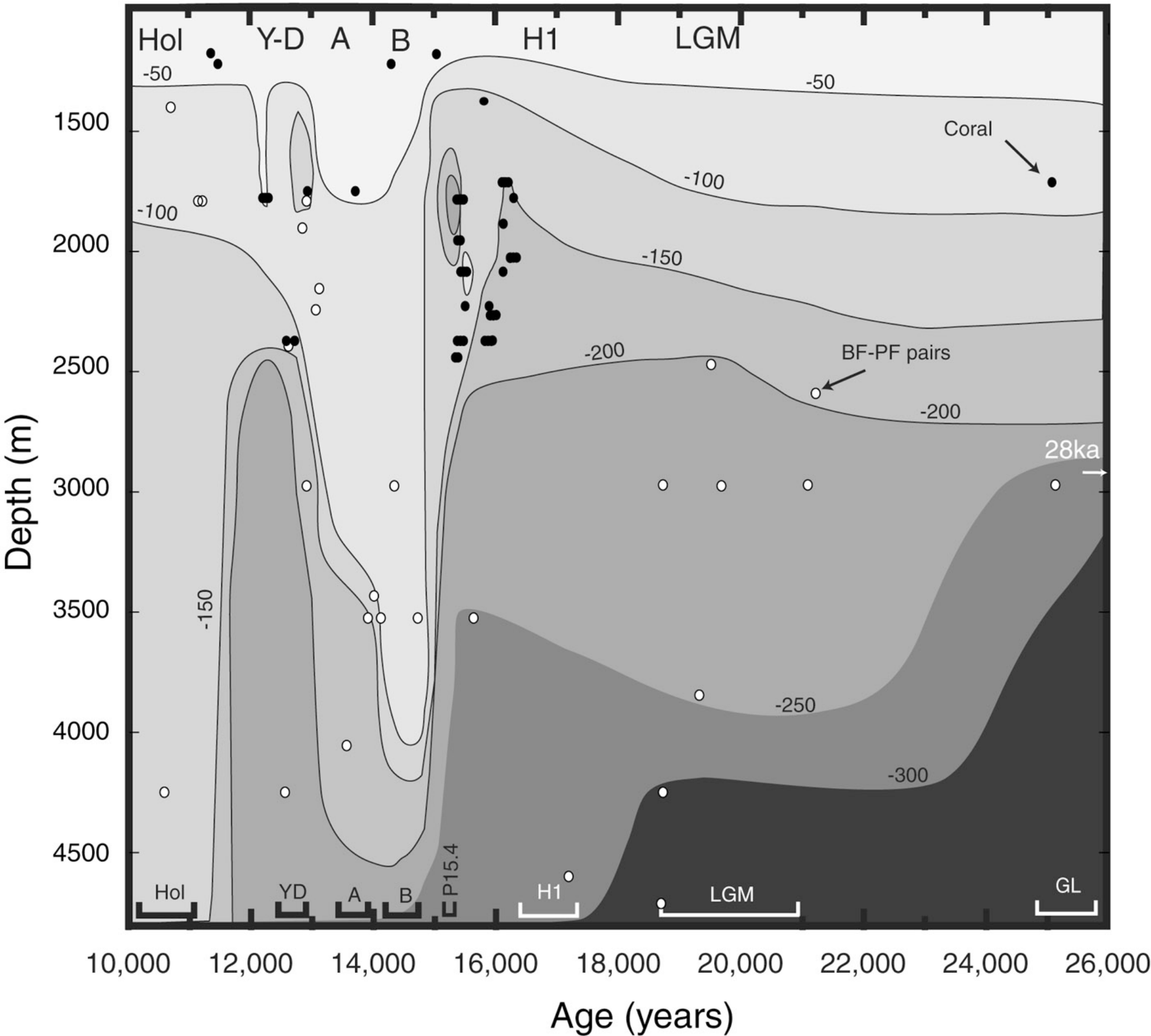
Hol
Y-D
A
B
H1
LGM
-50
-100
-150
-200
-250
-300
Coral
BF-PF pairs
28ka
P15.4
GL
Depth (m)
1500
2000
2500
3000
3500
4000
4500
10,000
12,000
14,000
16,000
18,000
20,000
22,000
24,000
26,000
Age (years)

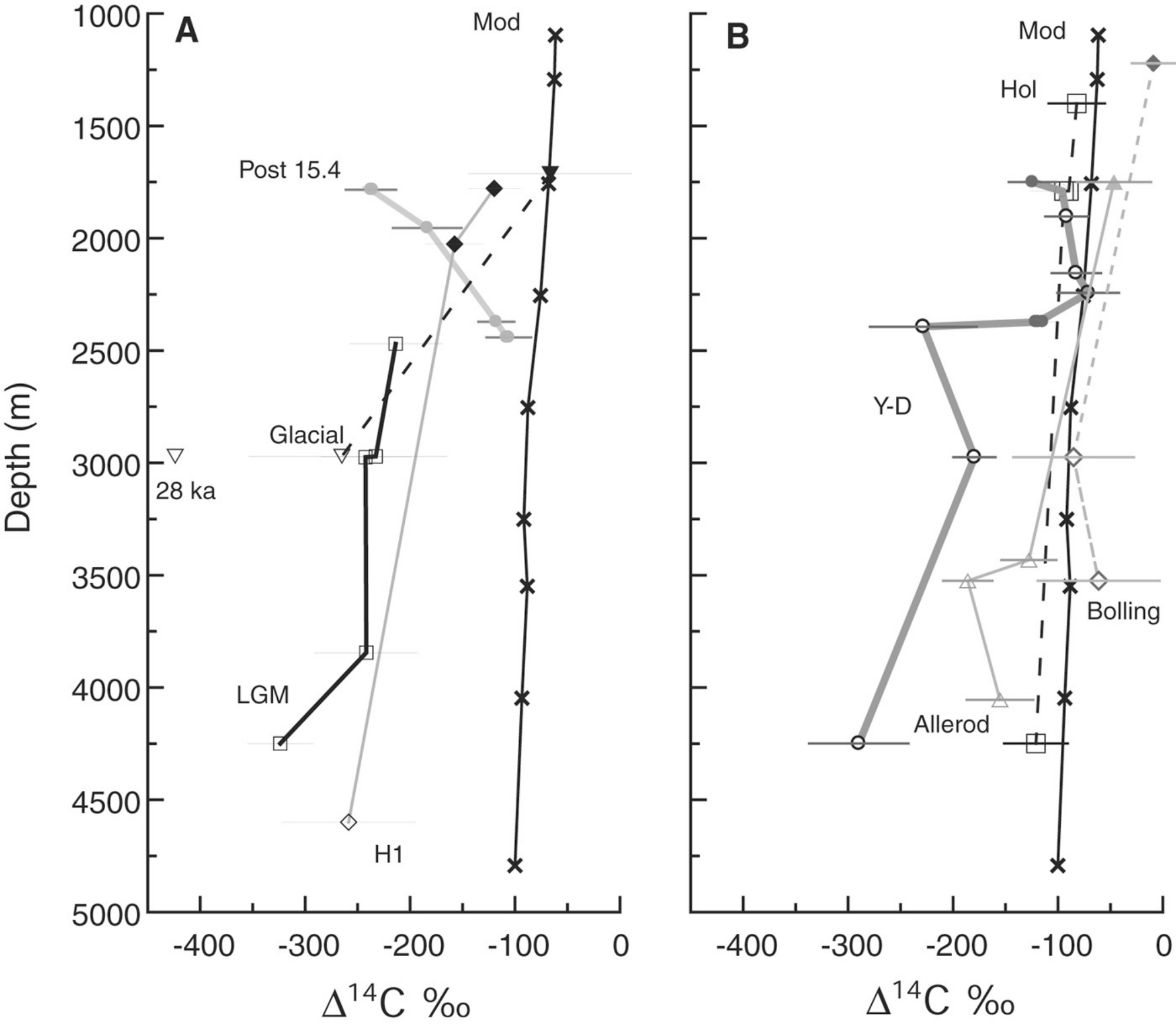
A
B
Mod
Post 15.4
Glacial
28 ka
LGM
H1
Hol
Y-D
Bolling
Allerod
Depth (m)
1000
1500
2000
2500
3000
3500
4000
4500
5000
-400
-300
-200
-100
0
Δ14C ‰